International Journal of Pharmaceutics 641 (2023) 123062

Contents lists available at ScienceDirect

International Journal of Pharmaceutics

journal homepage: www.elsevier.com/locate/ijpharm

Evaluation of a PAT-based in-line control system for a continuous spin freeze-drying process

Laurens Leys [*,1], Gust Nuytten[1], Pieter-Jan Van Bockstal, Thomas De Beer

Laboratory of Pharmaceutical Process Analytical Technology, Department of Pharmaceutical Analysis, Ghent University, 9000 Ghent, Belgium

ARTICLE INFO

Keywords:
Continuous manufacturing
Freeze-drying
Spin freeze-drying
PAT
NIR

ABSTRACT

Continuous spin freeze-drying provides a range of opportunities regarding the implementation of several in-line process analytical technologies (PAT) to control and optimize the freeze-drying process at the individual vial level. In this work, two methods were developed to (1) control the freezing phase by separately controlling the cooling and freezing rate and (2) control the drying phase by controlling the vial temperature (and hence the product temperature) to setpoint values and monitoring the residual moisture content. During the freezing phase, the vial temperature closely followed the decreasing setpoint temperature during the cooling phases, and the crystallization phase was reproducibly controlled by regulating the freezing rate. During both primary and secondary drying, vial temperature could be maintained on the setpoint temperature which resulted in an elegant cake structure after every run. By being able to accurately control the freezing rate and the vial temperature, a homogeneous drying time (SD = 0.07–0.09 h) between replicates was obtained. Applying a higher freezing rate significantly increased primary drying time. On the other hand, fast freezing rates increased the desorption rate. Finally, the residual moisture of the freeze-dried formulation could be monitored in-line with a high accuracy providing insight on the required length of the secondary drying phase.

1. Introduction

The process of freeze-drying is a well established technique in the pharmaceutical industry, especially for the drying of biopharmaceuticals. An estimated 34% of the currently marketed biopharmaceutical products needs to be freeze-dried in order to stabilize the product and make storage and distribution possible at room temperature (Gervasi et al., 2018). The conventional batch freeze-drying process consists of three stages. Firstly, during the freezing phase the product is frozen and cooled down to temperatures between −40 °C and −60 °C by means of temperature controlled shelves on which the entire batch of vials is placed. Next, primary drying is initiated by lowering the pressure in the drying chamber to pressures between 50 to 200 μbar and increasing the shelf temperature. During this phase the ice crystals, which were formed during the freezing phase, are removed by sublimation. Finally, when all ice is removed, the temperature of the product is increased by further increasing the shelf temperature to remove the unfrozen water during a secondary drying phase. During this phase, the unfrozen water that is bound onto or dissolved in the solutes is removed by desorption. In the end, a dried porous cake is obtained with a low residual moisture content which is typically below 1–3%, depending on the formulation (Kessler et al., 2015; Nail et al., 2002).

In 2004, the FDA released its "Framework for Innovative Pharmaceutical Development, Manufacturing, and Quality Assurance". According to these guidelines, process analytical technologies (PAT) should be implemented in pharmaceutical processes to enhance process understanding and to control the manufacturing process. This results in product quality that is built in by design (i.e., quality-by-design, QbD) as opposed to quality that is tested at the end of the manufacturing process (FDA, 2004). As outlined in a review by Patel et al., PAT may be implemented into the freeze-drying process at every phase of the process. For instance, thermocouples can be used to track the product temperature during the freezing and drying stages, Tunable Diode Laser Absorption Spectroscopy (TDLAS) can be utilized to conduct real-time sublimation rate measurements and NIR spectroscopy can be used to track the progress of secondary drying (Kauppinen, 2013; Patel and Pikal, 2009). However, freeze-drying of pharmaceuticals is conventionally performed as a batch process in which products are loaded and unloaded into and from the drying chamber as a single batch. This results in challenges when trying to adhere to the above mentioned FDA guideline. For one, it is usually difficult to measure more than a few selected vials with some PAT tools. These selected vial may not always be representative of the entire batch (e.g., vials with

* Corresponding author.
E-mail addresses: Laurens.Leys@UGent.be (L. Leys), Thomas.DeBeer@ugent.be (T. De Beer).
[1] These authors contributed equally to this work.

https://doi.org/10.1016/j.ijpharm.2023.123062
Received 24 February 2023; Received in revised form 11 May 2023; Accepted 13 May 2023
Available online 18 May 2023

thermocouples). Additionally, measurement techniques such as TDLAS provide information on the batch as a whole, but information on the single-vial level is often missing. Due to these reasons, it is challenging to ensure the quality of every vial in the batch (Patel and Pikal, 2009). Next to these issues, batch freeze-drying is associated with some disadvantages which have proven difficult to overcome such as long drying times, inhomogeneous sublimations rates and high deviations of residual moisture content between vials. In addition, up-scaling the entire process has proven to be difficult and time-consuming (Patel and Pikal, 2011; Pisano et al., 2013).

To address these challenges, an alternative freeze-drying technology for unit doses was proposed by Corver et al. namely continuous spin freeze-drying (Corver, 2013). In this process, the formulation is frozen by using a sterile cold gas with temperatures between −5 °C and −80 °C while spinning the vial between 2000 and 6000 rpm. This creates a thin layer of frozen formulation on the walls of the vial. As a consequence of the greatly increased surface area and thin product layer, primary drying times can be reduced by more than 90% as was shown in earlier research (De Meyer et al., 2015; Leys et al., 2020). Due to these reduced drying times, a continuous production process can be obtained by separating the freezing and drying chambers and connecting them by load locks to make transfer of vials possible from atmospheric pressure to vacuum. This continuous movement of vials offers opportunities for the implementation of various PAT tools for monitoring and controlling the quality of each vial. Furthermore, the process can be adjusted by implementing feedback mechanisms into each step of the process. In this work, the principles of the FDA guidance document were applied to the single vial unit (SVU), which is an R&D simulation system for continuous freeze-drying. Hereto, a control system for all process stages (freezing, primary and secondary drying) was developed using in-line PAT systems i.e., a thermocouple, an IR temperature sensor and an NIR probe for measuring residual moisture content. The goal of this approach is to control and optimize the freeze-drying process in-process at the single vial level and to homogenize drying times between vials. In addition, this approach, if proven effective, could act as a platform system for up-scaling the spin freezing process to a fully continuous freeze-drying system with minimal effort. Therefore, to determine the validity of the approach regarding these aspects, an experimental evaluation was performed using varying process conditions.

2. Materials and methods

2.1. Formulation

As a model formation, a solution of 33.3 mg/ml bovine serum albumin (BSA)(Sigma-Aldrich, Saint-Louis, USA) and 66.6 mg/ml sucrose (Sigma-Aldrich, Saint-Louis, USA) was prepared in deionized water. Aliquots of 4 ml of this formulation were transferred to type 1 tubular glass 10R vials (Schott, Müllheim, Germany).

2.2. Freeze-drying microscopy

Freeze-drying microscopy (FDM) was performed to determine the collapse/critical temperature (T_c) of the model formulation. Approximately 2 µl of the formulation was pipetted into the sample holder of a BX51 FDM cryo stage (Olympus, Hamburg, Germany) which was mounted on a FDCS 196 freeze-drying microscope (Linkam, Surrey, UK). The sample was frozen by decreasing the temperature of the sample to −40 °C (50 °C/min) using the Linksys32 software. Next, sublimation was started by decreasing the pressure inside the cryo stage to 2 Pa using a rotary vane vacuum pump (E2M1.5, Edwards, Nazareth, Belgium). After an equilibration period of 1 min, temperature of the cryo stage was gradually increased every 2 min in steps of 1 °C. Digital microscopy images were taken just before raising the temperature of the sample. T_c was defined as the first temperature at which slight alterations were visible in the dried layer structure compared to previous images.

2.3. NIR calibration for in-line residual moisture determination

2.3.1. Sample preparation

A total of 70 samples were spin frozen (using a rate of heat transfer during crystallization of 3.6 W) and subsequently freeze-dried using varying process conditions to create samples with different moisture contents. After spin freezing, all 70 samples were equally distributed across the five pre-cooled shelves of a EPSILON 2-10D LSCPLUS freeze dryer (Martin Christ, Osterode am Harz, Germany) in aluminium holders. Primary drying was performed overnight using a shelf temperature of −30 °C and a chamber pressure of 10 Pa. After primary drying was complete, samples on the lowest shelf were stoppered and the chamber was aerated so that the stoppered samples could be removed. The drying chamber was subsequently evacuated and shelf temperature increased to decrease the moisture content of the remaining samples. This process was repeated until all vials were stoppered and removed from the chamber. The shelf temperatures that were used for this process were −30, −20, −10, 10 and 40 °C and the time between every aeration step was 2 h.

2.3.2. Near infrared spectroscopy

A predictive multivariate NIR model for the residual moisture was developed with spectra recorded using a SentroPAT NIR spectrometer (Sentronic GmbH, Dresden, Germany) which was implemented in-line in an SVU prototype (Rheavita, Belgium, Zwijnaarde). The 70 dried samples were transferred one by one to the SVU prototype in which 10 NIR spectra per sample were taken under vacuum (7 Pa) while rotating at a speed of 5 rpm. The integration time and the averaging number were respectively 10 ms and 125. Spectra were recorded in a spectral range between 1100 and 2200 nm.

2.3.3. Karl Fischer titration

A Karl Fischer titration was performed via external extraction principle on all 70 samples to determine the residual moisture content. Hereto, the freeze-dried product was reconstituted with a known volume of a 1:1 methanol/formamide (both Sigma-Aldrich, Saint Louis, MO, USA) mixture and left to equilibrate for roughly 15 min. With the help of a syringe, a known volume of this solution was removed from the vial, injected in the titration vessel of the Mettler Toledo V30 volumetric Karl Fischer titrator (Schwerzenbach, Switzerland) and titrated with Hydranal® titration solvent (Sigma-Aldrich, Saint Louis, MO, USA). Prior to the measurement of the residual water, the concentration of the titration solvent and the moisture content of the dry methanol was determined in triplicate.

2.3.4. Multivariate calibration of moisture content using NIR spectra

The NIR spectral data (X, 700 spectra: 10 spectra per sample) were linked to the measured residual moisture content (Y, 70 moisture contents: 1 moisture content per sample from Karl Fischer analysis) by fitting the following simple multiple linear model to the data:

$$Y = X\beta + \epsilon \quad (1)$$

In order to derive the coefficients (β) for the model, an elastic net regularization algorithm was applied. The collected NIR spectra were pre-processed using a Savitsky–Golay (SG) smoothing followed by standard normal variate (SNV) transformation. Of the dataset, 80% of the samples were randomly chosen and used for calibration. The remaining 20% was used for external validation. To measure the performance of the model leave-one-out cross-validation was used. During this cross-validation, all 10 spectra of 1 specific sample were consecutively left out while fitting the model on the remaining data, after which a root-mean-square error of cross-validation (RMSEcv) could be calculated using the left out spectra. A root-mean-square error of prediction (RMSEP) value was calculated based on predictions of the external validation dataset. Multivariate calibration was performed using the scikit-learn package version 1.0.2 in Python version 3.9.16.

2.4. Development of PAT-controlled feedback algorithms

Two control algorithms for controlling the spin freeze-drying process were programmed in LabVIEW using proportional integral (PI) control: one for the spin freezing process and another for the subsequent drying stages (i.e., primary drying and secondary drying). The goal of these algorithms is to obtain uniform process conditions and uniform optimal drying times for all continuously freeze-dried samples without exceeding the collapse temperature. Therefore the following formula, which describes the sublimation rate during primary drying, needs to be considered:

$$\dot{m} = \frac{A_p(P_i - P_c)}{R_p} \tag{2}$$

where $\dot{m}$ is the sublimation rate (kg/s), A_p is the area of the sublimation interface (m^2), P_i is the partial water vapour pressure at the sublimation front and P_c is the chamber pressure during primary drying (Pa). R_p is the dried product layer resistance (m/s) which is related to the size and shape of pores within the dried product, formed by sublimation of ice crystals formed during the crystallization phase. It follows from this formula that the drying rate between vials can be homogenized if the following conditions are met:

1. The pressure difference between the sublimation front and the chamber is kept constant. This can be done by keeping both the chamber pressure and the product temperature at the sublimation front at a fixed value since T_i is related to P_i by the Clausius–Clapeyron Equation:

$$P_i = 3.6 \times 10^{12} e^{-\frac{6145}{T_i}} \tag{3}$$

2. R_p is homogenized between vials. The R_p depends on the pore structure of the product, which depends on the size of the ice crystals formed during the freezing phase. It has been shown that the ice crystal size and the resulting R_p depends on both the amount of supercooling and the freezing rate during the freezing step (Nakagawa et al., 2007). Considering this, it can be assumed that a reproducible and controlled way of freezing will lead to a reproducible pore structure. In this work, the freezing rate during the spin freezing phase was controlled, while nucleation remained uncontrolled, in order to control the resulting R_p during drying. Please note the difference between cooling rate and freezing rate. As discussed below, freezing rate refers to the amount of heat transferred during the crystallization phase of freezing. Cooling rate refers to the rate of temperature change during the phases before and after the crystallization phase.

Note that these algorithms were developed for the SVU system in which one vial can be dried at a time. This system is therefore used as a simulation system of a continuous process. It can be hypothesized that if both freezing rate and product temperature during drying is controlled in the same way as in the SVU, similar drying times between those systems will be observed. A more in detail explanation of the control algorithms can be found in the sections below, while the used PI control law and PI parameters can be found in supplementary material (S1, S2).

2.4.1. Spin freezing

The spin freezing phase was controlled by using a combination of a mechanistic freezing model and a PI control of the cold gas flow, a system adapted from previous work (Nuytten et al., 2021).

The control system is based on two separate sets of tubings (Fig. 1A). One set of tubing passes through room temperature air, while the other passes through a liquid nitrogen heat exchanger, resulting in cooled gas. The cold and room temperature gasses mix, whereafter the resulting gas passes through a gas diffuser. Before hitting the rotating vial, the gas temperature is measured by a type T thermocouple. Gas flow through both gas tracks is controlled using two mass flow controllers (F-202AV-M20, Bronkhorst). Spin freezing consists of three separate phases: liquid cooling, crystal growth and solid cooling. A dedicated control strategy was used for each of these phases.

During liquid cooling, the product is present in a liquid form and cools down until nucleation occurs. In this phase, vial temperature was measured using a FLIR A655sc IR camera. To this end, a square region of interest was chosen on the vial, and the vial temperature was defined as the mean temperature of all pixels in this square. This approach was used in previous work where the vial temperature was measured during spin freeze-drying (Van Bockstal et al., 2018). The input signals for the proportional integral (PI) control system are the vial temperature and the dynamic temperature setpoint, of which the latter depends on the set cooling rate. These input signals were used to calculate a gas flow rate (i.e., the PI output) using manually determined PI parameters. Criteria for optimization of PI parameters included fast response time, low steady state systematic error and stability around the setpoint. A PI controller was chosen because simple proportional control resulted in a systematic steady state error which required integral control action to correct. No excessive overshoot of the setpoint was observed and control performance was sufficient using only PI control, so no D (i.e., derivative) term was used.

The gas flow calculated using the PI controller is the setpoint of the mass flow controller of the cooled gas track, while the valve of the other flow controller remains closed during the liquid cooling phase. In this way, the product cools down at the required cooling rate until the nucleation temperature is reached.

Nucleation is a process whereby the first ice crystals are formed within the liquid formulation, which results in a sharp product temperature and turbidity increase. This sharp increase in temperature was used as a trigger for the LabVIEW virtual instrument to proceed to the next phase of spin freezing.

During the crystal growth phase, the ice nuclei formed during nucleation grow until most liquid water has crystallized. The rate at which these ice crystals grow is proportional to the amount of heat transferred from the vial towards the cooling gas per time unit, which is expressed as $\dot{Q}$ (W). $\dot{Q}$ may be calculated using the Fourier law of heat conduction (Nuytten et al., 2021):

$$\dot{Q} = \pi h \varnothing_{vial} h_{vial} (T_{v,o} - T_{gas}) \tag{4}$$

Where h is the heat transfer coefficient ($W/(m^2K)$), $\varnothing_{vial}$ is the outer diameter of vial (m), h_{vial} is the height of vial (m), $T_{v,o}$ is the temperature at the outside of the vial wall (K) as measured by the IR camera and T_{gas} (K) is the temperature of the cooling gas as measured by the thermocouple. h is related to the efficiency of heat transfer of the cooling system and was calibrated using the gas flow rate, as was described previously (Nuytten et al., 2021). In this work, calibration experiments were performed using a constant total gas flow rate $\dot{V}_{total}$ of 100 L/min during the crystallization phase. Hereto, a calibration experiment at this flow rate was performed in triplicate to determine h at the start of every day where an experiment was performed.

In order to achieve a desired $\dot{Q}$, the required gas temperature $T_{gas,setpoint}$ was calculated using the following equation:

$$T_{gas,setpoint} = T_{v,o} - \frac{\dot{Q}}{h \varnothing_{vial} h_{vial}} \tag{5}$$

The cooling gas temperature was controlled by varying the gas flow rates of the mass flow controllers while keeping the total gas flow rate constant (i.e., at 100 L/min). To this end, the calculated gas temperature was used as input for a second PI control system. In this system, the gas temperature setpoint calculated from Eq. (5) is used along with the measured gas temperature to calculate the required gas flow rate of the mass flow controller responsible for the cold gas flow $\dot{V}_{cold}$. As the total gas flow rate $\dot{V}_{total}$ is constant, the corresponding gas flow rate of the mass flow controller responsible for the room temperature gas flow $\dot{V}_{warm}$ is calculated as follows:

$$\dot{V}_{warm} = \dot{V}_{total} - \dot{V}_{cold} \tag{6}$$

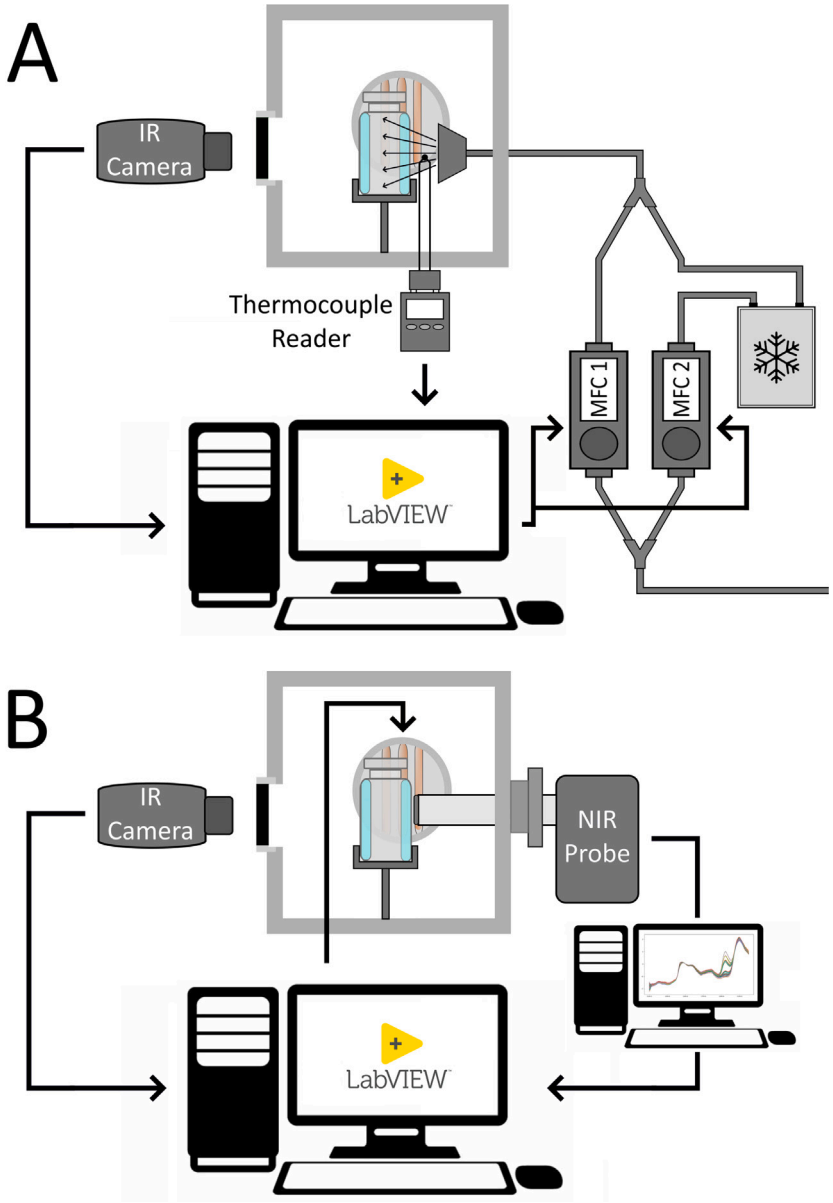

Fig. 1. Schematic representation of the control loop setup. A: Control of the freezing phase. The cooling gas travels from a gas source towards two flow controllers. Mass flow controller 1 (MFC 1) outputs gas into tubings at room temperature, while gas from MFC 2 passes through a liquid nitrogen heat exchanger. Both gas flows subsequently mix and pass through a gas diffuser before exposing the rapidly rotating vial to gas of a controlled temperature and flow rate. The vial and gas temperature are measured by an infrared (IR) camera and a thermocouple, respectively. These sensors provide inputs for a LabVIEW virtual instrument which provides a gas flow rate setpoint to the mass flow controllers. B: Control of the drying phase. IR heaters provide heat for the sublimation of ice and desorption of bound water within the slowly rotating vial. An IR camera continuously measures the vial temperature, and a near infrared (NIR) probe records NIR spectra of the product within the vial. The IR camera provides the input for a LabVIEW virtual instrument which determines a voltage setpoint for the IR heaters.

The rate of heat transfer $\dot{Q}$ was sustained until the crystallization phase was completed. To determine the end of the crystallization phase, the duration of the crystallization phase t_{cryst} was calculated:

$$t_{cryst} = \frac{Q_{cryst}}{\dot{Q}} \tag{7}$$

With Q_{cryst} the heat released due to the crystallization of the vial contents (J), excluding any ice crystallized during nucleation, and $\dot{Q}$ the mean rate of heat transfer during the crystallization phase (W). Further details regarding the calculation of t_{cryst} may be found in our previous work (Nuytten et al., 2021).

After t_{cryst} has elapsed, the solid cooling phase is initiated. The control system during this phase is the same as the one during the liquid cooling phase, using PI control with a dynamic vial temperature setpoint and measured gas flow rates as input.

2.4.2. Primary and secondary drying

The drying control algorithm was separated in 3 consecutive parts, i.e, primary drying, a transition phase from primary to secondary drying, and secondary drying. All three phases were controlled by a closed loop system to maintain vial temperature at the desired setting. The input for the closed loop sytem was provided by two PAT systems, i.e. the IR camera to measure vial temperature during the entire process and the SentroPAT NIR spectrometer to measure the residual moisture content during the secondary drying phase. Data communication between the SentroPAT embedded PC and the remote PC, running the LabVIEW program, was achieved by an open communications platform (OPC) server interface. During the process the vial is rotated at 5 rpm so that all PAT systems could provide information on the entire vial. As in the freezing phases, a square region of interest was chosen on

the vial for temperature measurement, and the vial temperature was defined as the mean temperature of all pixels in this square.

During the primary drying phase, a PI control mechanism was implemented in the LabVIEW virtual instrument which adjusted the voltage setpoint of a voltacraft PPS-16005 power source based on the IR camera vial temperature measurement. The power source was connected to the IR-heaters of the SVU to maintain vial temperature at the desired setpoint (see Section 2.5). Note that the IR camera measures the temperature at the outside of the vial and not at the sublimation front. By using the temperature at the outside of the vial, an extra safety margin is built in as the product temperature at the inside of the vial is always colder than the temperature at the outside. This temperature gradient could however be calculated using Fourier's law of heat conduction, as was described in previous work, and is usually in the range of 1 to 2 °C (Leys et al., 2020). Again a manually tuned PI system was chosen (i.e., contrary to a P or PID controller) for the same reasons as with the freezing control system, and with the same optimization criteria. Additionally, during the primary drying phase an important factor regarding the control system is preventing the vial temperature from exceeding the collapse temperature. In this way, excessive overshoots of the controller must be avoided.

To detect the endpoint of primary drying and the start of the transition phase, fluctuations in vial temperature across the rotating vial wall were monitored. as soon as ice sublimation is completed at a certain location of the vial, the heat sink which is the sublimation process disappears. The product in the vial will therefore naturally heat up at that point creating temperature differences across the vial. To avoid overheating of these locations, the IR-heaters are automatically switched off for the remainder of the primary drying process. For this purpose, a standard deviation for vial temperature was calculated from the 20 last consecutive time points (= 20 LabVIEW virtual instrument loop iterations). When this deviation was higher than 1.5 °C, the heaters were switched off. The endpoint of the entire primary drying process was defined as the moment where the lowest temperature measurement of these 20 consecutive time points was above −20 °C. This approach makes it possible to identify the point in the vial where sublimation finishes last due to the rotation of vial in front of the IR camera.

During the transfer phase from primary to secondary drying, the product slowly heats up to the environmental temperature. A heating ramp can be set in the LabVIEW virtual instrument to speed up this phase, which creates a dynamic temperature setpoint. Again, the vial temperature is controlled by means of PI control of the IR-heaters. Since the wall temperature of the SVU prototype was not controlled for this work, the minimum heating rate is between 3–4 °C/min. During all experiments, the ramp was set to 1 °C/ min, meaning that the heaters were turned off for the entire phase which makes it as conservative as possible. This point will be further elaborated in the discussion. The transfer phase is considered finished when the vial reaches the final setpoint value of the secondary drying process temperature. The vial temperature is then fixed at the final setpoint for the remaining time of the secondary drying process.

Product moisture content was continuously measured by using the received spectra from the in-line NIR probe. These spectra were pre-processed by the LabVIEW virtual instrument in the same way as was done during calibration of the NIR moisture determination method, and the moisture content was derived using Eq. (1). Therefore, it was possible to follow up the moisture content in-line during the process and evaluate desorption kinetics. The secondary drying process could be stopped either when a desired moisture content was reached or a preset time limit was exceeded.

2.5. Experimental evaluation of the algorithm and effect of process settings

In order to evaluate if the developed PAT based continuous freeze-drying control methodology as described in Section 2.4 holds, several freezing and drying scenarios were evaluated. To determine the impact of the freezing protocol, two freezing rates were compared of which the slow and fast freezing rate corresponded respectively to a $\dot{Q}$ of 3.6 W and 20 W. For each freezing rate, 3 replicates were performed to demonstrate that the PAT based control methodology is able to achieve homogeneous drying rates between the replicates. The cooling rate for both liquid and solid cooling phase was set to 20 °C/min. After reaching −50 °C, primary drying was initiated by lowering the pressure to 7 Pa. For these runs the primary drying vial temperature was fixed at −28 °C, 1 °C below the collapse temperature of the formulation. The vial temperature during secondary drying was set at 30 °C.

To demonstrate the effect of controlling the primary drying vial temperature on the primary drying rate, 3 different vial temperatures for primary drying were selected (i.e., −30 °C, −28 °C and −22 °C) of which one was above the collapse temperature to assess the impact on the cake structure. During the freezing phase of these three experiments, liquid and solid cooling rate was set to 20 °C/min while $\dot{Q}$ was set to 3.6 W, corresponding to a low freezing rate. The chamber pressure was fixed at 7 Pa and the final secondary drying temperature was 30 °C. The total drying duration of all runs was fixed to 3.5 h in order to make a fair comparison between runs. A summary of the performed experiments for algorithm validation can be found in Table 1.

Table 1
Summary of algorithm validation experiments. All experiments were performed with a cooling rate of 20 °C/min for both the liquid and solid cooling phase and a secondary drying temperature of 30 °C. Experiments 1–3 and experiments 4–6 are replicates.

Experiment number	Freezing Rate (W)	Primary drying temperature (°C)	Results section
1	20	−28	3.2, 3.4
2	20	−28	3.2, 3.4
3	20	−28	3.2, 3.4
4	3.6	−28	3.2, 3.3, 3.4
5	3.6	−28	3.2, 3.4
6	3.6	−28	3.2, 3.4
7	3.6	−22	3.3
8	3.6	−30	3.3

2.6. Scanning electron microscopy

Scanning electron microscopy (SEM)(Quanta 200F, Thermo Fisher Scientific, Waltham, MA, USA) was used to evaluate the pore size and tortuosity of a cross section of the freeze-dried cakes. Per drying condition in Section 2.5, one vial was used to perform the analysis. All vials were carefully tapped against a bench to break up the cake so that a piece of dried cake could be placed on its side on the SEM sample holder. Each sample was coated with a 40 nm gold layer using a sputter coater (Quorum Technologies, Laughton, UK). Finally, images of the product were captured in the scanning microscope under high vacuum conditions.

2.7. Specific surface area determination

Argon adsorption was used to determine the specific surface area as calculated from sorption data using the BET equation. To this end, samples were degassed for 16 h at 50 °C prior to measurement. Degassed samples were loaded into glass tubes and placed into a 3P micro 200 automatic volumetric sorption device. Argon isotherms were acquired at 87 K and BET calculations were performed in a P/P_0 range of 0.10–0.30. The specific surface area was measured from samples of experiment numbers 1,2,4,5 and 7 (see Table 1). Experiment 7 was repeated to yield an additional sample. In this way, two samples per condition were measured.

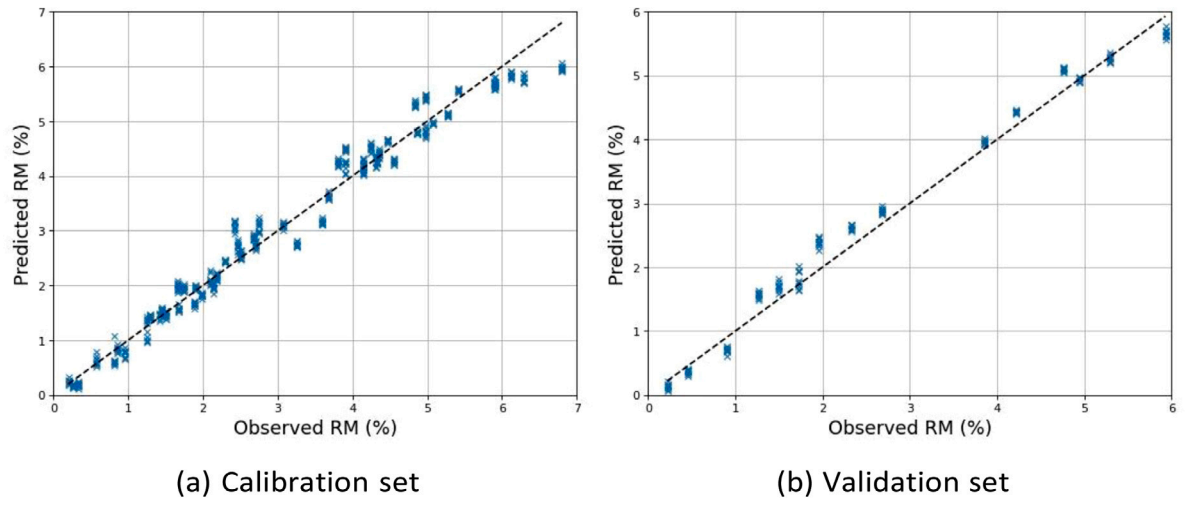

Fig. 2. Observed versus predicted residual moisture plots using the obtained coefficients for the multivariate linear model.

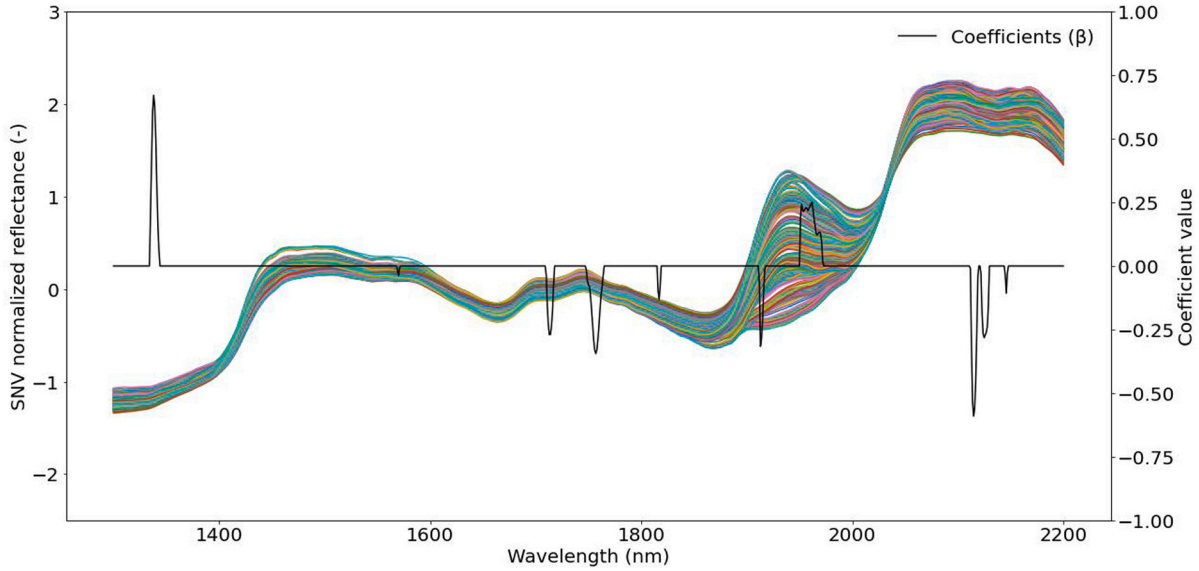

Fig. 3. Overlay of smoothed and SNV filtered spectra of the calibration set with the obtained coefficients for the linear regression model to predict the residual moisture content.

3. Results

3.1. NIR calibration model

The residual moisture content of the calibration samples that were used for NIR model calibration model ranged between 0.2 and 6.8%. As can be seen from Fig. 2, a good correlation between observed residual moisture content and NIR model based predicted moisture content was obtained for both calibration and validation samples. The obtained RMSEcv and RMSEP for the calibration samples and validation samples was respectively 0.27 and 0.23%. The accuracy of the model was therefore deemed acceptable for determining the rate of desorption during secondary drying.

In Fig. 3, an overlay between the obtained coefficients for the multivariate model and the NIR spectra of the calibration samples is shown. From this, it can be observed that the model is selective for residual moisture as the most important wavelength regions, selected by the elastic net algorithm, correspond well with the -OH bend–stretch combination bands of water at 1940 nm. Additional selected regions are also correlated to this wavelength region since the strong NIR signal of water highly influences the SNV filtering which was applied to the sample spectra inducing information of this wavelength region into the other regions (1350 nm, 1600–1850 nm).

3.2. Impact of freezing rate on pore structure, cake appearance and primary drying rate

The control algorithm for the freezing process was able to control all phases of the freezing process and provide reproducible results as can be seen from Figs. 4 and 6. The quality of the freezing process control was assessed using three runs at high freezing rate, and three runs at low freezing rate (see Section 2.6). Here, during the liquid cooling phase, the mean offset error was on average −0.06 °C, while the average of the standard deviation on the offset error was 0.28 °C. For slow freezing, the endpoint temperature of the freezing process was reached in 8.8 ± 0.5 min (mean ± SD, $n = 3$) after nucleation, for fast freezing it was reached in 1.3 ± 0.1 min after nucleation.

Macroscopic cake appearance and SEM images for different freezing rates are shown in Fig. 5. To this end, samples were used from experiment numbers 1,4 and 7 (see Table 1). From close visual inspection, a small effect of the freezing rate could be observed on the cracking phenomena which is also sometimes observed after batch freeze-drying and

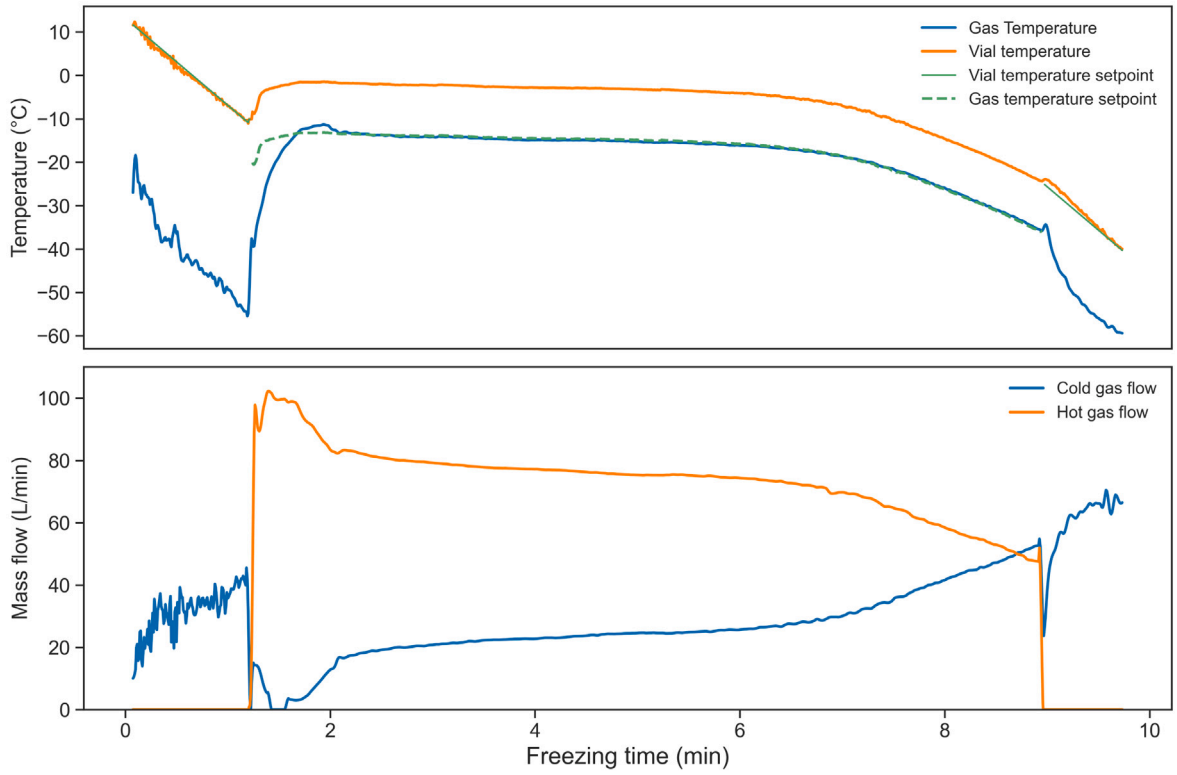

Fig. 4. Vial temperature (including setpoint), gas temperature (including setpoint) and mass flows during the freezing phase of a slowly frozen sample.

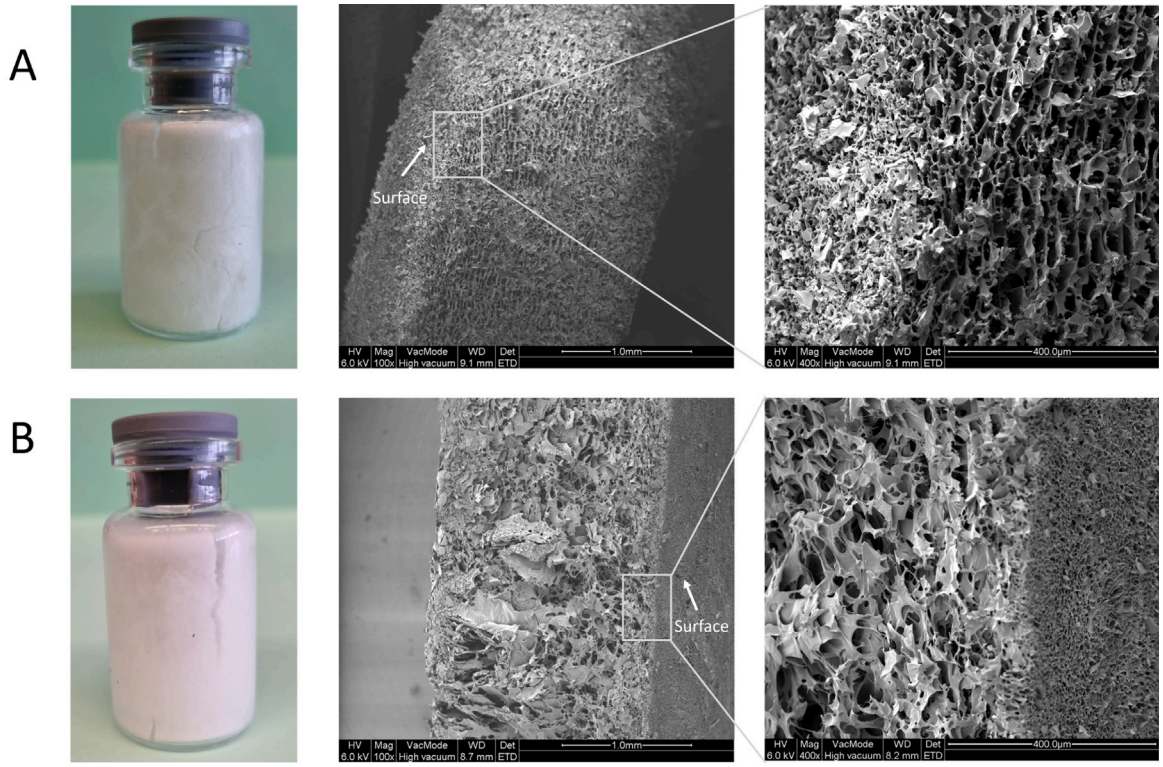

Fig. 5. Cake quality (left) and SEM image analysis (middle and right). A: Sample frozen at a low freezing rate. B: Sample frozen at a high freezing rate.

which is dependent on the formulation composition (Ullrich, 2014). Slowly frozen samples generally had smaller and more cracks distributed over the entire dried structure than fast frozen samples. On the other hand, the cake structure of fast frozen samples usually contained a smaller amount of larger cracks. After further inspection, no other defects could be observed. SEM image analysis showed however that the freezing rate had a significant effect on pore structure. When a slow freezing rate was used, the pore structure appeared to be more

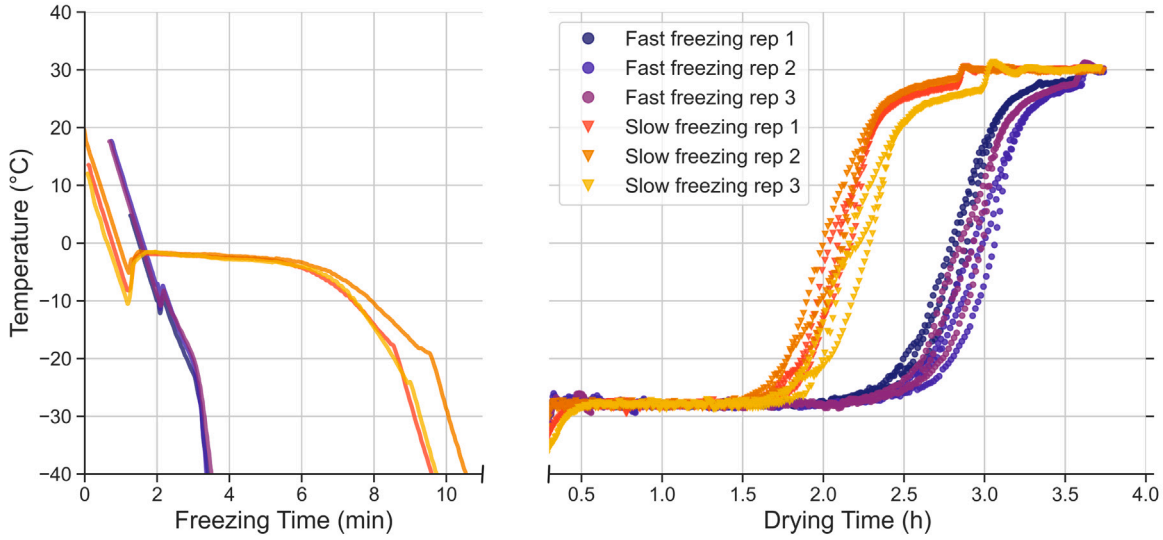

Fig. 6. Vial temperature over time for 3 representative spin freeze-drying cycles per freezing rate (Run 1–6).

homogeneous while a more tortuous structure was obtained during fast freezing. Due to this tortuous structure of the fast frozen samples, it is difficult to compare the size of the pores between freezing rates. It is however noteworthy to point out that the pores at the (inner) surface of the cake of the cylinder appeared to be more narrow for fast frozen samples.

Concerning the impact of freezing on drying rate, it can be observed from Fig. 6 that freezing rate was strongly correlated to primary drying duration. The primary drying time for slow freezing was 1.78 ± 0.07 h (mean ± SD, $n = 3$), and the primary drying time for fast freezing was 2.47 ± 0.09 h.

3.3. Evaluation of vial temperature control and the effect on primary drying time

As an example of the drying control mechanism, the data of a representative drying run (i.e., corresponding to experiment number 5, Table 1) is plotted in Fig. 7. From this figure it can be observed that the vial temperature was tightly controlled at the setpoint level for both primary (−28 °C) and secondary drying (30 °C) (Figure S3). For the three runs in which vial temperature was varied (i.e., corresponding to experiment numbers 4, 7 and 8, Table 1), the mean offset error between the setpoint vial temperature and measured vial temperature was on average 0.30 °C below the setpoint. The average standard deviation of the offset error was 0.43 °C. In addition, the collapse temperature, which was determined to be −27 °C by FDM, was never exceeded during primary drying for both runs where the primary drying setpoint temperature was set below the collapse temperature (i.e., experiment numbers 4 and 7, Table 1). At the end of primary drying and during the transition phase, there is a sharp increase of the vial temperature. Since the endothermic process of sublimation is completed at this point, radiation from the surrounding chamber walls can only be used for heating up the product which explains the steep rise in temperature during the transition phase. During the transition phase, it can be observed that the power of the heaters was automatically switched off and the endpoint of primary drying was correctly detected by the control algorithm. Since the natural rise in temperature due to radiation during the transition between primary and secondary drying is faster than this ramp, the setpoint control mechanism is only visible at the end of the transition phase when the ramp catches up with the natural heating of the product.

To demonstrate the impact of vial temperature during primary drying on the sublimation rate, 3 different vial temperature settings (i.e., −22 °C, −28 °C and −30 °C) were evaluated. One setting was specifically set above the collapse temperature to determine the effect on cake structure if this temperature was exceeded. The vial temperatures and primary drying time duration for each run are plotted in Fig. 8. As expected, the primary drying time decreased with increasing set vial temperature. The sublimation rate approximately increased by 24% by increasing the vial temperature setpoint from −30 °C to −28 °C. Surprisingly, drying above the collapse temperature did not cause any noticeable issues during primary drying as no macroscopic defects were observed and an intact cylindrical cake structure was still obtained. However, SEM image analysis showed signs of microcollapse in some parts of the cake in the form of merged pores as can be seen in Fig. 9.

3.4. Impact of freezing rate on secondary drying kinetics and specific surface area

In Fig. 10, the secondary drying kinetics of samples frozen at varying freezing rates are compared. Furthermore, the desorption profile of the sample dried above the collapse temperature has been included. Note that the desorption profiles in this figure are plotted from the endpoint of primary drying, which is different for each freezing rate and therefore each sample. The observation was made that desorption kinetics were slower for samples that were frozen using a slow freezing rate compared to those that were frozen rapidly. As a result, after 3.5 h of total processing time (primary + secondary drying), a residual moisture content of 1.45 ± 0.19% (mean ± SD, $n = 3$) was measured for slowly frozen samples while for fast frozen samples a residual moisture content of 1.18 ± 0.1% was obtained. These values were obtained by NIR measurements and were confirmed by KF analysis which showed a mean absolute deviation from the NIR prediction of only 0.13%. Note that, while this difference in residual moisture content between the two freezing rates is statistically insignificant ($p = 0.0949$), primary drying finished later for the fast frozen samples, which resulted in a shorter secondary drying time as compared to slowly frozen samples (i.e., ± 45 min shorter). Nonetheless, relatively low moisture contents were achieved for all samples after only 1.7 and 0.6 h of secondary drying time, respectively for slow and fast freezing methods. For the sample that was dried above the collapse temperature during primary drying, slower desorption kinetics were observed as compared to the

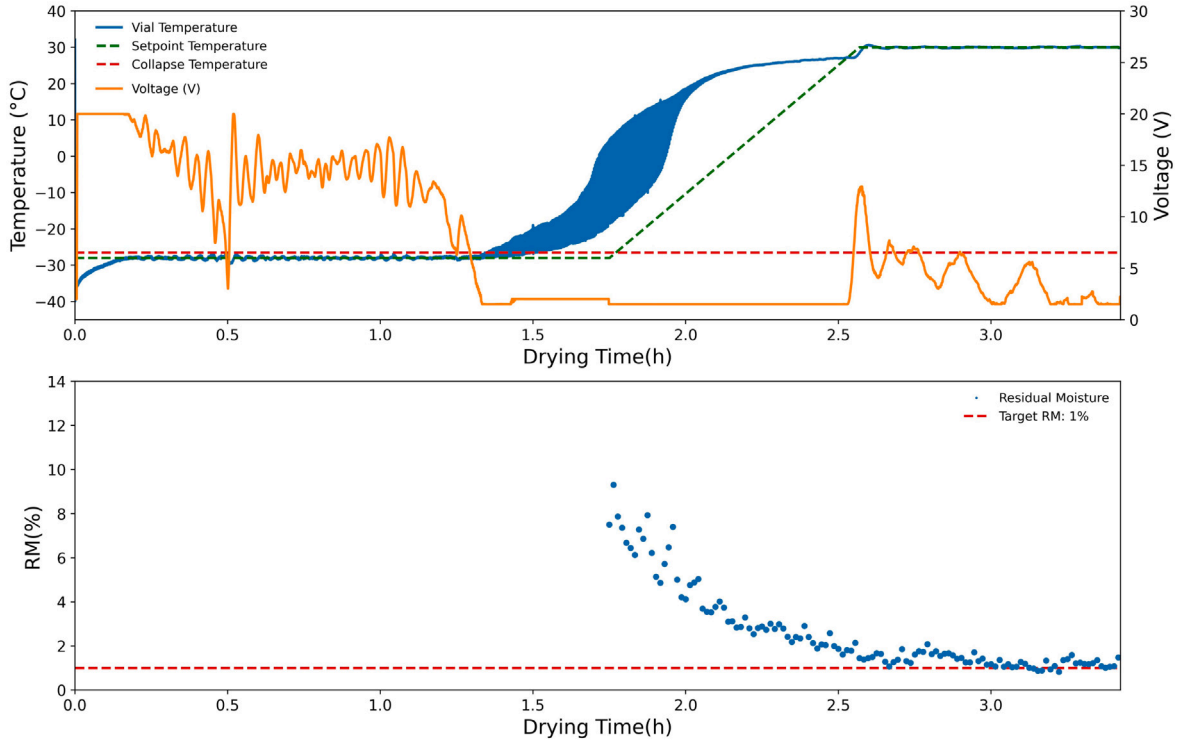

Fig. 7. Vial temperature and residual moisture content over time for a representative sample (experiment 5, see Table 1). Residual moisture (RM) target, voltage of the IR heaters, vial temperature setpoint and collapse temperatures are indicated.

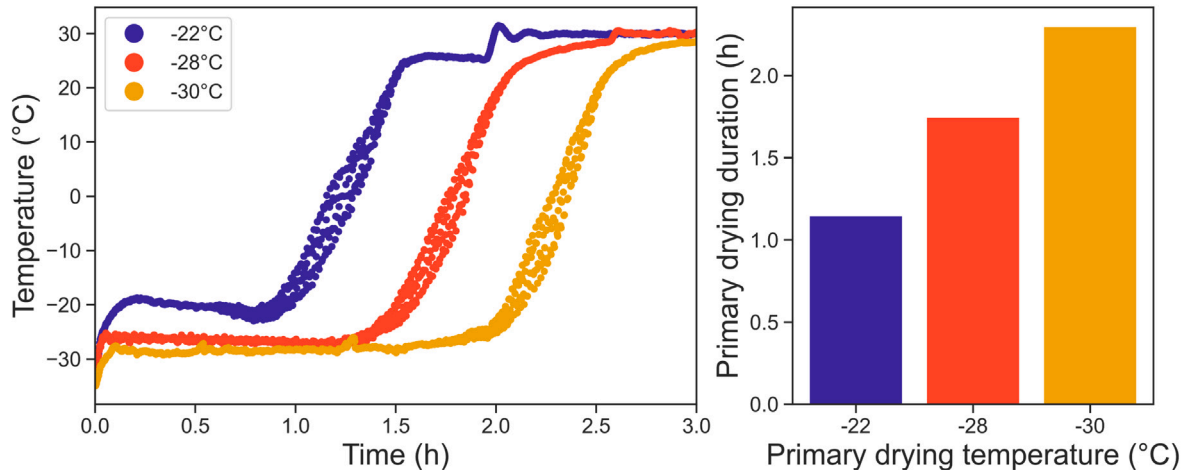

Fig. 8. Vial temperature over time and primary drying duration for varying primary drying temperatures (Run 6–8). The end of primary drying is associated with a sharp increase in vial temperature.

other samples. In addition, a relatively high moisture content of 1.61% was obtained for this sample after almost 2 h of secondary drying. Interestingly, these results correlated nicely with the specific surface area measurements by BET (Fig. 10, S4). Using a slower freezing rate significantly decreased the specific surface area of the dried product. For the (micro-)collapsed sample an even lower surface area was reported. It can therefore be argued that a higher specific surface area leads to faster desorption rates and a lower residual moisture content at the end of the process.

4. Discussion

In this work, a PAT-based control strategy for continuous spin freeze-drying was presented. The theory of this approach, described in Section 2.4, proved to be a sound basis for the control of all steps in the continuous freeze-drying process.

Firstly, results show that by controlling the crystallization rate during the freezing phase, R_p can be sufficiently homogenized between vials to ensure equal sublimation rates, despite the lack of controlled nucleation methods. Note that this approach differs from the batch freezing method were only the cooling rate of the shelves can be controlled. In a batch freeze-drying process, the shelves cool down continuously to a final temperature during the freezing phase. Hence, the time of nucleation (i.e., the degree of supercooling) determines the temperature difference between the bottom of the vial and the shelf, which in turn determines the rate of heat transfer during crystallization. In this way, the uncontrolled nucleation also creates an uncontrolled and heterogeneous freezing rate in a batch freeze-drying process. In

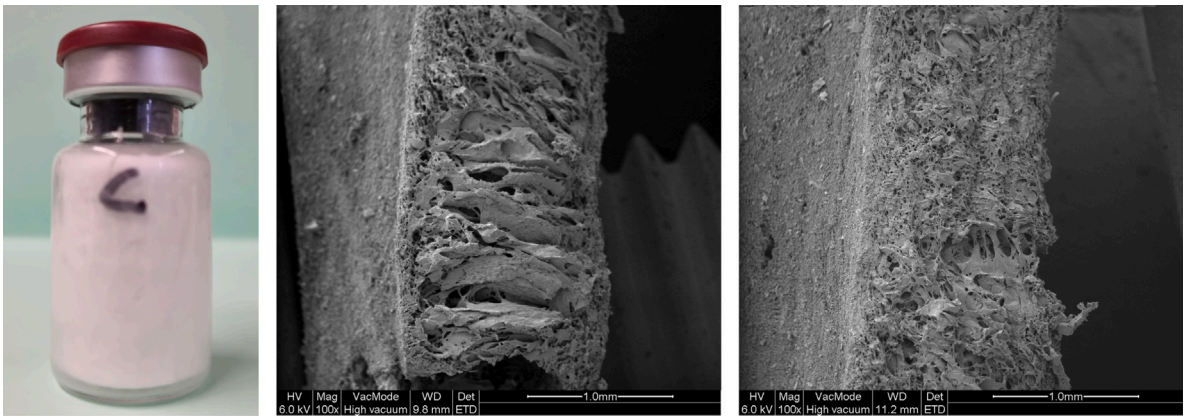

Fig. 9. Cake quality (left) and SEM image analysis (middle and right). The sample was generated using a high freezing rate and a primary drying temperature of −22 °C.

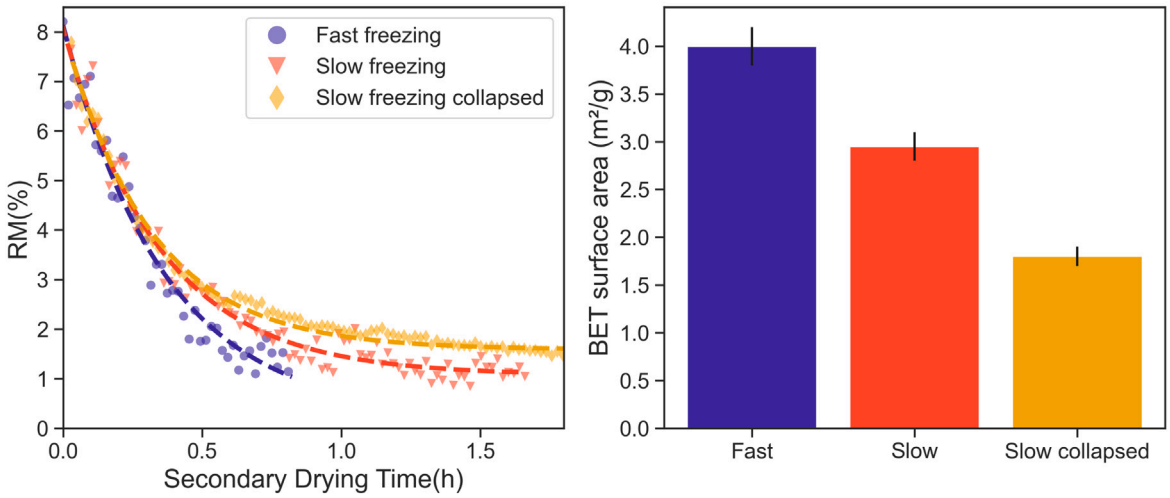

Fig. 10. Secondary drying kinetics in function of freezing rate. Fast and slow freezing conditions were dried at a primary drying temperature of −28 °C. The slowly frozen collapsed condition was dried at a primary drying temperature of −22 °C, which is 5 °C above the collapse temperature. Three representative desorption profiles including an empirical fit through the data (i.e., as indicated by the dashed line) for a fast and slowly frozen sample are indicated on the left. The mean specific surface area for each freezing condition is shown on the right. Error bars indicate the standard deviation ($n = 2$).

contrast, during spin freezing, the freezing rate depends on the controllable temperature difference between the vial and the cooling gas. This temperature difference can be immediately adjusted at the point of nucleation, contrary to the shelves of a batch freeze-dryer (Nuytten et al., 2021). By keeping the temperature difference between vial and cooling gas constant, a constant and controlled freezing rate can be achieved during spin freezing. In this way, the amount of supercooling may not be as impactful for spin freezing, as the freezing front velocity remains the same, regardless of the amount of supercooling. This may also explain the relatively low variability of drying times as a result of spin freezing, while a range of nucleation temperatures were obtained (i.e., as seen in Fig. 6).

Furthermore, while it was expected that using different freezing rates would have an effect on the sublimation rate, the reduction in primary drying time for slowly frozen samples was surprisingly high (> 27%, around 45 min). This highlights the relevance of the control algorithm for the freezing phase. Indeed, in order to homogenize drying rates between the vials, it is not sufficient to control the water vapour pressure difference between the sublimation front and the chamber during the primary drying phase. This partial approach would only exacerbate differences in drying time by not considering the differences in R_p. It has been described in literature that an increase in freezing front velocity is linked to smaller ice crystals during batch freeze-drying (Nakagawa et al., 2007; Oddone et al., 2017). In this way, it can be expected that a faster freezing rate as in these experiments will lead to a faster moving freezing front. In turn, this would lead to smaller ice crystals. During primary drying, these small ice crystals result in small pores left behind after sublimation, which results in a relatively high R_p and consequently in an increased primary drying time. While this theory could not directly be observed from the SEM images, an alternative theory can be suggested. The increase in pore tortuosity for fast frozen samples could hamper the ability of water molecules to leave the product. In addition, fast freezing seemed to decrease the pore size at the inner surface of the cylinder, potentially creating a barrier or increased resistance from the start of sublimation. Concerning secondary drying, it is generally accepted that the freezing rate impacts this step as well. Indeed, as mentioned above, the freezing phase impacts the subsequent pore structure of the freeze-dried cake and therefore the specific surface area of the dried layer. Here, we can reason that fast freezing results in small pores with a large overall surface area, which was confirmed by BET-analysis, and therefore increases the desorption rate (Oddone et al., 2017). This means that it is important to maintain pore structure during all phases of the drying process. Indeed, if the collapse temperature is exceeded at any point during the drying process, this can lead to differences in residual moisture content between samples. This was clearly the case for the sample which was dried above the collapse temperature. While no macroscopic defects were observed, signs of microcollapse were present

on the SEM image and a decrease in desorption kinetics was observed compared to a sample using the same freezing rate but dried below the collapse temperature.

Secondly, using a closed loop control system for the drying phase can indeed speed up the drying process while maintaining product quality. In addition, the sublimation rates between vials, which are dried by using the same vial temperature setpoint, can be homogenized using this approach. Interestingly, observed deviations from the mean primary drying time between vials, which were processed using the same freezing an drying conditions, are only in the range of 4 to 6 min. These deviations from the mean drying rate are extremely small compared to vials in a batch freeze-drying process, where values in the range of hours were reported (Oddone et al., 2016; Kauppinen, 2013). While for batch freeze-drying induced nucleation can mitigate differences in R_p between vials, it cannot correct for the excess radiation from the walls on the vials situated at the edge of the shelves, which increases the product temperature (Pisano et al., 2007). One study where the heterogeneity of primary drying rate in a batch freeze-drying process was measured found a coefficient of variation ranging from 5% to 12% (Searles et al., 2001). In this work, on the other hand, approximate values of 5% and below were consistently found for both fast (i.e., a standard deviation of 4.2 min) and slow (i.e., a standard deviation of 5.4 min) freezing rates. This indicates that the low absolute values for the variation of sublimation rate can only be partially attributed to the short drying times and that the drying algorithm can correct for other sources of variation such as small deviations in environmental temperature. Note that for a continuous freeze-drying process, homogeneous drying times are essential as they ensure a continuous output of material without needing to change the processing speed of the system.

The presented control strategy approach clearly provides some possibilities compared to the standard way of process optimization which often uses mechanistic modelling to calculate an optimal design space. Various mechanistic models of the 3 phases (freezing, primary drying and secondary drying) were published over the years for both continuous and batch freeze-drying processes. However due to the various assumptions and large uncertainty on parameters such as R_p, usability is often limited (Van Bockstal et al., 2017). The variability of drying rates between vials makes it difficult to guarantee product quality for every vial and at the same time optimize drying rates. In other words, the obtained optimal process settings will tend to be over-conservative for a large part of the batch in the best scenario (Pisano et al., 2007). Furthermore, optimized process settings have to be calculated for every new formulation and cannot be directly transferred to a larger scale. Using PAT tools such as IR temperature measurement systems and NIR probes provide accurate real-time information on the product, eliminating the uncertainty on the R_p and other parameters. Note that in a continuous system it is not feasible to implement NIR probes on the entire line to get information on the moisture content over time. The SVU unit however can be used to simulate the drying process in a continuous freeze-dryer, acting as a platform system for easy up-scaling. Instead of transferring process settings to a larger scale system, a product/vial temperature profile can be transferred. In addition, using this method of up-scaling only requires information on the collapse temperature and not on specific values for R_p or heat transfer coefficients (K_v) for different scales of freeze-dryers. Indeed, the algorithms developed in this work automatically take the influence of these parameters into account by measuring the vial temperature. Here, the assumption is made that if the product temperature profile between SVU and continuous freeze-dryer is identical (regulated by PI), the sublimation rate and the moisture content will likewise also be identical. Nonetheless, this hypothesis remains to be validated and should be investigated once a fully continuous system with process control becomes available in the future.

While the results of the developed PAT-based continuous freeze-drying process control method are promising, there are some shortcomings which need to be addressed. Since the spinning of the vial and intra-vial ice sublimation are not completely homogeneous, primary drying does not finish at all points of the vial at the same time (Goethals et al., 2020). This results in a relatively broad band (i.e., 15–20 min) of temperature values that persists until after the complete sublimation of ice. Before reaching the secondary drying setpoint temperature, the temperature within the product homogenizes, indicated by a narrow band of temperature values. In addition, the minimum temperature ramp which can be achieved by the current system is rather high which can lead to (micro-)collapse for certain formulations with lower T_g' values. An efficient solution would be to cool the walls of the system and hence control the wall temperature, allowing to set a slower ramp during the transfer phase and minimizing the risk for collapse. In this case, the ramp up phase could be modified by implementing the Gordon Taylor equation:

$$T_g = \frac{w_1 T_{g,w} + k w_2 T_{g,s}}{w_1 + k w_2} \tag{8}$$

in which w_1 and w_2 are the respective weight fractions of moisture and solutes. $T_{g,w}$ and $T_{g,s}$ are the glass transition temperatures of water and dried solid (RM = 0%). k is a calibration constant which can be determined by means of DSC. The T_g, which increases in function of the decreasing residual moisture, can be calculated in real-time allowing the set a dynamic product temperature profile during the transfer phase to avoid exceeding this temperature.

5. Conclusion

Using feedback control algorithms for the different stages of the continuous spin freeze-drying process proved to be highly effective to regulate the drying process of the product in the SVU. By using these algorithms the influence of freezing rate on both sublimation and desorption rate can be reliably be controlled. In addition, an optimized primary drying trajectory can quickly be obtained with only a limited amount of information (i.e., the critical temperature). In a next step, optimized product temperature profiles should be validated in a fully operational continuous spin freeze-drying system in order to test the transferability of the approach.

CRediT authorship contribution statement

Laurens Leys: Conceptualization, Methodology, Software, Formal analysis, Investigation, Writing – original draft, Writing – review & editing. **Gust Nuytten:** Conceptualization, Methodology, Software, Formal analysis, Investigation, Writing – original draft, Writing – review & editing. **Pieter-Jan Van Bockstal:** Conceptualization, Software, Writing – review & editing. **Thomas De Beer:** Conceptualization, Resources, Writing – review & editing, Supervision.

Declaration of competing interest

The authors declare the following financial interests/personal relationships which may be considered as potential competing interests: Pieter-Jan Van Bockstal reports financial support was provided by Flanders Innovation & Entrepreneurship. Pieter-Jan Van Bockstal reports a relationship with RheaVita that includes: employment. Thomas De Beer reports a relationship with RheaVita that includes: board membership, employment, and equity or stocks.

Data availability

Data will be made available on request.

Acknowledgements

Financial support for this research from the Flanders Innovation & Entrepreneurship (VLAIO - Innovation mandate HBC.2017.0534 - Postdoctoral fellowship P.-J.V.B.), Belgium is gratefully acknowledged.

The authors would like to thank Andreas Laemont from the Centre for Ordered Materials, Organometallics and Catalysis (COMOC, Ghent university) for conducting the specific surface area measurements and subsequent data analysis.

Appendix A. Supplementary data

Supplementary material related to this article can be found online at https://doi.org/10.1016/j.ijpharm.2023.123062.

References

Corver, Jos, 2013. Method and system for freeze-drying injectable compositions. In: Particular Pharmaceutical. WO2013036107.

De Meyer, L., Van Bockstal, P.-J., Corver, J., Vervaet, C., Remon, J P, De Beer, T, 2015. Evaluation of spin freezing versus conventional freezing as part of a continuous pharmaceutical freeze-drying concept for unit doses. Int. J. Pharm. 496 (1), 75–85. http://dx.doi.org/10.1016/j.ijpharm.2015.05.025, (ISSN: 1873-3476 (Electronic)).

FDA, 2004. U. S. Food and Drug Administration. Guidance for industry: PAT—a framework for innovative pharmaceutical development, manufacturing, and quality assurance. September. URL: http://www.fda.gov/downloads/Drugs/GuidanceComplianceRegulatoryInformation/Guidances/ucm070305.pdf.

Gervasi, V., Dall Agnol, R., Cullen, S., McCoy, T., Vucen, S., Crean, A., 2018. Parenteral protein formulations: An overview of approved products within the European Union. Eur. J. Pharmaceut. Biopharmaceut. (ISSN: 0939-6411) 131, 8–24. http://dx.doi.org/10.1016/j.ejpb.2018.07.011, URL: https://www.sciencedirect.com/science/article/pii/S0939641117314789.

Goethals, Wannes, Vanbillemont, Brecht, Lammens, Joris, De Beer, Thomas, Vervaet, Chris, Boone, Matthieu, 2020. In-situ X-ray imaging of sublimating spin-Frozen solutions. Materials 13, 2953. http://dx.doi.org/10.3390/ma13132953.

Kauppinen, Ari, 2013. In-line multipoint near-infrared spectroscopy for moisture content quantification during freeze-drying. ISBN: 9789526117171.

Kessler, William, Sharma, Puneet, Mujat, Mircea, 2015. Advances in Instrumental Analysis Applied to the Development of Lyophilization Cycles. ISBN: 978-1-4939-2382-3, pp. 43–72. http://dx.doi.org/10.1007/978-1-4939-2383-0_4.

Leys, L., Vanbillemont, B., Van Bockstal, P.J., Lammens, J., Nuytten, G, Corver, J, Vervaet, C, De Beer, T, 2020. A primary drying model-based comparison of conventional batch freeze-drying to continuous spin-freeze-drying for unit doses. Eur. J. Pharmaceut. Biopharmaceut. (ISSN: 18733441) 157 (September), 97–107. http://dx.doi.org/10.1016/j.ejpb.2020.09.009.

Nail, S.L., Jiang, S., Chongprasert, S., Knopp, S.A., 2002. Development and manufacture of protein pharmaceuticals. In: Steve, L. Nail, Michael, J. Akers (Eds.), Fundamentals of Freeze-Drying. Pharmaceutical Biotechnology. Vol. 14. Springer, Boston, MA.

Nakagawa, Kyuya, Hottot, Burélie, Vessot, Séverine, Andrieu, Julien, 2007. Modeling of freezing step during freeze-drying of drugs in vials. AIChE J. (ISSN: 00011541) 53 (5), 1362–1372. http://dx.doi.org/10.1002/aic.11147.

Nuytten, Gust, Revatta, Susan Ríos, Van Bockstal, Pieter Jan, Kumar, Ashish, Lammens, Joris, Leys, Laurens, Vanbillemont, Brecht, Corver, Jos, Vervaet, Chris, De Beer, Thomas, 2021. Development and application of a mechanistic cooling and freezing model of the spin freezing step within the framework of continuous freeze-drying. Pharmaceutics (ISSN: 19994923) 13 (12), http://dx.doi.org/10.3390/pharmaceutics13122076.

Oddone, Irene, Barresi, Antonello A., Pisano, Roberto, 2017. Influence of controlled ice nucleation on the freeze-drying of pharmaceutical products: the secondary drying step. Int. J. Pharm. (ISSN: 0378-5173) 524 (1), 134–140. http://dx.doi.org/10.1016/j.ijpharm.2017.03.077, URL: https://www.sciencedirect.com/science/article/pii/S0378517317302648.

Oddone, Irene, Van Bockstal, Pieter-Jan, De Beer, Thomas, Pisano, Roberto, 2016. Impact of vacuum-induced surface freezing on inter- and intra-vial heterogeneity. Eur. J. Pharmaceut. Biopharmaceut. (ISSN: 0939-6411) 103, 167–178. http://dx.doi.org/10.1016/j.ejpb.2016.04.002, URL: https://www.sciencedirect.com/science/article/pii/S0939641116301266.

Patel, Sajal Manubhai, Pikal, Michael, 2009. Process analytical technologies (PAT) in freeze-drying of parenteral products. Pharm. Dev. Technol. 14 (6), 567–587. http://dx.doi.org/10.3109/10837450903295116, (ISSN: 1097-9867 (Electronic)).

Patel, Sajal Manubhai, Pikal, Michael J., 2011. Emerging freeze-drying process development and scale-up issues. AAPS PharmSciTech 12 (1), 372–378. http://dx.doi.org/10.1208/s12249-011-9599-9, (ISSN: 1530-9932 (Electronic)).

Pisano, Roberto, Fissore, Davide, Barresi, Antonello A, Brayard, Philippe, Chouvenc, Pierre, Woinet, Bertrand, 2013. Quality by design: optimization of a freeze-drying cycle via design space in case of heterogeneous drying behavior and influence of the freezing protocol. Pharm. Dev. Technol. 18 (1), 280–295. http://dx.doi.org/10.3109/10837450.2012.734512, (ISSN: 1097-9867 (Electronic)).

Pisano, Roberto, Fissore, Davide, Barresi, Antonello A, Chimica, Ingegneria, Torino, Politecnico, 2007. Heat transfer in freeze-drying apparatus. J. Phys. Chem..

Searles, James, Carpenter, John, Randolph, Theodore, 2001. Annealing to optimize the primary drying rate, reduce freezing-induced drying rate heterogeneity, and determine Tgín pharmaceutical lyophilization. J. Pharm. Sci. 90, 872–887. http://dx.doi.org/10.1002/jps.1040.

Ullrich, Sabine, 2014. Quantitative Measurements of Shrinkage and Cracking During Freeze-Drying of Amorphous Cakes (Ph.D. thesis).

Van Bockstal, Pieter-Jan, Corver, Jos, De Meyer, Laurens, Vervaet, Chris, De Beer, Thomas, 2018. Thermal imaging as a noncontact inline process analytical tool for product temperature monitoring during continuous freeze-drying of unit doses. Anal. Chem. 90 (22), 13591–13599. http://dx.doi.org/10.1021/acs.analchem.8b03788, PMID: 30339362.

Van Bockstal, Pieter-Jan, Mortier, Séverine Thérèse F C, Corver, Jos, Nopens, Ingmar, Gernaey, Krist V, De Beer, Thomas, 2017. Quantitative risk assessment via uncertainty analysis in combination with error propagation for the determination of the dynamic Design Space of the primary drying step during freeze-drying. Eur. J. Pharmaceut. Biopharmaceut. Official J. Arbeitsgemeinschaft Fur Pharmazeutische Verfahrenstechnik E.V 121, 32–41. http://dx.doi.org/10.1016/j.ejpb.2017.08.015, (ISSN: 1873-3441 (Electronic)).